

RESEARCH ARTICLE | MAY 02 2025

Observation of the interaction between Au^- and CO_2 in $\text{Au}(\text{CO}_2)_n^-$ anions: Physisorption as the dominant mechanism



Zonghui Guo; Shihu Du ; Wei Huang ; Wenbao Zhao; Haiyan Han ; Zhi Zhao ; Yongliang Yan ; Zhihui Fan ; Ruili Shi ; Hua Xie ; Ling Jiang

Check for updates

J. Chem. Phys. 162, 174310 (2025)

<https://doi.org/10.1063/5.0265399>



Articles You May Be Interested In

Non-classical hydrogen storage mechanisms other than chemisorption and physisorption

Appl. Phys. Rev. (June 2022)

Effect of van der Waals interactions on the chemisorption and physisorption of phenol and phenoxy on metal surfaces

J. Chem. Phys. (September 2016)

Transformation from chemisorption to physisorption with tube diameter and gas concentration: Computational studies on NH_3 adsorption in BN nanotubes

J. Chem. Phys. (November 2007)



The Journal of Chemical Physics
**Special Topics Open
for Submissions**

[Learn More](#)

Observation of the interaction between Au^- and CO_2 in $\text{Au}(\text{CO}_2)_n^-$ anions: Physisorption as the dominant mechanism

Cite as: J. Chem. Phys. 162, 174310 (2025); doi: 10.1063/5.0265399

Submitted: 13 February 2025 • Accepted: 17 April 2025 •

Published Online: 2 May 2025



View Online



Export Citation



CrossMark

Zonghui Guo,¹ Shihu Du,^{2,3} Wei Huang,¹ Wenbao Zhao,¹ Haiyan Han,¹ Zhi Zhao,^{1,3,a)}
Yongliang Yan,^{1,a)} Zhihui Fan,¹ Ruili Shi,^{1,a)} Hua Xie,^{3,a)} and Ling Jiang³

AFFILIATIONS

¹School of Mathematics and Physics Science and Engineering, Hebei Computational Optical Imaging and Photoelectric Detection Technology Innovation Center, Hebei International Joint Research Center for Computational Optical Imaging and Intelligent Sensing, Hebei University of Engineering, Handan 056038, China

²School of Chemistry and Chemical Engineering, Shandong University, Jinan 250100, China

³State Key Laboratory of Molecular Reaction Dynamics, Dalian Institute of Chemical Physics, Chinese Academy of Sciences, Dalian 116023, China

^{a)}Authors to whom correspondence should be addressed: zhaozhi@hebeu.edu.cn; yylhhy@163.com; shiruili@hebeu.edu.cn; and xiehua@dicp.ac.cn

ABSTRACT

In this study, we investigated the structure and bonding of $\text{Au}(\text{CO}_2)_n^-$ ($n = 2, 3$) using photoelectron spectroscopy analysis, quantum chemical calculations, and weak interaction analysis. Quantum chemical calculations revealed that the geometries of the physisorbed structures closely aligned with experimental data, suggesting that these configurations were the most stable under the experimental conditions. Conversely, while chemisorbed structures exhibit stronger interactions and considerable CO_2 activation, they show less agreement with the observed spectroscopic data. Using the interaction region indicator method, our weak interaction analysis confirmed that van der Waals forces were the dominant interaction in the physisorbed structures. Our experimental results indicate that these physically adsorbed structures are more stable under the conditions of this study. These findings shed light on the interaction mechanisms of $\text{Au}(\text{CO}_2)_n^-$ ($n = 2, 3$) at the molecular level and provide new insights into the potential for transition metals to catalytically activate CO_2 .

Published under an exclusive license by AIP Publishing. <https://doi.org/10.1063/5.0265399>

INTRODUCTION

The increasing concentration of atmospheric CO_2 is driving global warming and sea level rise, presenting considerable environmental challenges.^{1,2} Sequestration and conversion of CO_2 are considered crucial strategies for mitigating these issues. Furthermore, CO_2 's inherent carbon content makes it a valuable source of carbon. However, the thermodynamic stability and chemical inertness of CO_2 molecules hinder its conversion into valuable chemicals.^{3–8} One promising approach for activating and reducing CO_2 into desired energy products involves the formation of a bent, metastable

CO_2^- species upon electron acceptance. Most CO_2 conversion processes rely on metal-based catalysts.^{9,10} Transition metals stand out as promising candidates for CO_2 reduction reactions owing to their abundance of surface active sites and unique electronic structure and catalytic properties.¹¹ Transition metal atoms and clusters can form coordination compounds with CO_2 molecules, which changes the electronic distribution in CO_2 and lowers its reduction potential, facilitating activation.^{4,8,12–16} Understanding the binding motifs and molecular interactions of these active sites provides a simplified framework for elucidating the fundamental mechanisms of catalytic CO_2 activation.^{17,18} By investigating microscopic models

of metal–CO₂ composite clusters in a vacuum gas phase environment, we can effectively circumvent the complexities associated with the inherent heterogeneity of condensed phases. Research studies on transition metal cluster structures and reactivity offer detailed insights into their architecture. Spectroscopic techniques and quantum chemical calculations have been widely used to investigate interactions between carbon dioxide and metal atoms in the gas phase.^{8,19–23}

The interaction between bare metal atomic cations and CO₂ has been extensively studied over the past decades. Previous research using ion beam and infrared photodissociation techniques has consistently observed the formation of the M⁺–OCO structure during interactions between metal cations and carbon dioxide. These studies, encompassing cations such as V⁺, Ni⁺, Mg⁺, Fe⁺, Al⁺, Ca⁺, Co⁺, Rh⁺, and Ir⁺^{10,20,24–34} consistently demonstrate an M⁺–OCO arrangement. In this configuration, CO₂ acts as a weakly bound solvation molecule with a slightly positive charge. The metal cations form an end-on bond with the oxygen atom in CO₂, through a charge–quadrupole electrostatic interaction. This interaction results in a shortened C–O bond while maintaining a linear CO₂ subunit. In contrast to cations, anions bind to CO₂ through the carbon atom. This interaction induces deformation of the CO₂ molecule owing to electrostatic effects and charge transfer.³⁵ Weber and colleagues have reported monodentate coordination [M(η¹–CO₂)][−] for CO₂ interactions with M = Bi[−], Cu[−], Ag[−], and Au[−].^{15,36–38} They also observed a bidentate configuration [M(η²–CO₂)][−] for Co[−],³⁹ Ni[−],⁴⁰ and Mn[−].⁴¹ Miller's group further identified a bidentate complex [ClMg(η²–O₂C)][−].⁴²

Photoelectron spectroscopy studies by Bowen *et al.* have revealed distinct binding behaviors in transition metal–CO₂ anionic complexes, depending on the specific metal involved. Complexes featuring Cu[−], Ni[−], Pd[−], and Pt[−] anions demonstrate covalent bonding between the metal and CO₂ ligand, indicating a chemisorption mode.^{9,14} In these cases, a partial negative charge is transferred from the metal anion to the CO₂ moiety of the (M–CO₂)[−] complex, resulting in considerable bending of the CO₂ molecule. This bending suggests that CO₂ is activated by the negative charge transfer. In contrast, Ag[−] forms electrostatically bonded (physisorbed) anionic complexes with CO₂, where the CO₂ molecule exhibits only slight bending, indicating minimal CO₂ activation. Interestingly, both physisorption and chemisorption isomers exist for Au[−], denoted as Au[−](CO₂) and Au(CO₂)[−], respectively. These isomers exhibit very similar energies, which may explain their coexistence in experimental observations. However, compared to Cu[−], the chemisorption interaction between Au[−] and CO₂ is relatively weaker.¹⁴ The Zeng group reported that the main characteristic peaks in the photoelectron spectra of Au[−] exhibit significant shifts after interacting with different gas molecules, indicating that the gas molecules influence the electronic state of Au[−] through weak interactions.⁴³ The Bowen group, through analysis of the photoelectron spectra of Au[−] interacting with one or two water molecules, found that the positions and intensities of the spectral peaks exhibit a clear trend with the increasing number of water molecules.⁴⁴ While Weber's group has investigated the interactions of multiple CO₂ molecules with transition metal anions using infrared spectroscopy, only the Au(CO₂)_{*n*}[−] isomers with chemisorption characteristics were detected.³⁶

Photoelectron spectroscopy (PES) studies investigating the electronic structure and interactions in CO₂–transition metal anion systems are scarce. Understanding these interactions is critical for advancing research in areas such as catalysis and CO₂ activation. In our previous work, the reaction of Au[−] with CO₂ has been investigated by photoelectron velocity-map imaging,⁴⁵ and we found both physisorbed and chemisorbed structures on the spectra. In this study, we continue to investigate the photoelectron spectra of the anionic metal complexes Au(CO₂)_{*n*}[−] (*n* = 2, 3) in the gas phase. Theoretical calculations were performed to provide further insights into the coordination bonding between transition metal anions and CO₂ molecules. These calculations aim to analyze the reaction mechanism of anionic metal ions with CO₂ and explore the catalytic properties of the metal clusters.

EXPERIMENTAL METHODS

The experiments were performed using a custom-built laser vaporization source coupled with a dual-channel time-of-flight mass spectrometer. Detailed descriptions of this apparatus have been published elsewhere.⁴⁶ A small amount of CO₂ (5%) was introduced into the helium carrier gas in the laser sputtering source, which was used to vaporize the gold target and generate Au(CO₂)_{*n*}[−] (*n* = 2, 3). The carrier gas stagnation pressure was typically maintained at 2–5 atm. After cooling and expansion into the source chamber, the anions of interest were mass-selected using a Wiley–McLaren time-of-flight mass spectrometer and subsequently introduced into the photodetachment region, where they interacted with 355 nm (3.496 eV) laser beams. Photoelectrons were detected using a microchannel plate and phosphor screen assembly. The two-dimensional images produced on the phosphor screen were captured using a charge-coupled device camera. Each image was generated by accumulating 10 000–50 000 laser shots at a 10 Hz repetition rate. All raw images were reconstructed using the basis set expansion (BASEX) inverse Abel transform method. The experimental photoelectron spectra are mainly discussed in the article. The photoelectron spectra were calibrated against the known spectrum of Au[−]. The energy resolution achieved was better than 5%, corresponding to 50 meV at an electron kinetic energy of 1 eV.

COMPUTATIONAL DETAILS

To elucidate the geometrical and electronic structures of Au(CO₂)_{*n*}[−] (*n* = 2, 3), theoretical calculations were performed using Gaussian 09 program.⁴⁷ We conducted calculations on the target system using multiple functionals and basis sets to determine the relative energies of the isomers (see Table S1 of the [supplementary material](#)) and the VDE values ([supplementary material](#)). As shown in Tables S1 and S2, the relative energy differences calculated with different functionals are small; in particular, the M06-2X functional demonstrated the highest consistency with the experimental data and effectively characterized the physisorbed structures present in the system.

Therefore, structures were optimized using the M06-2X⁴⁸ functional, with the 6–311G+(3df)⁴⁹ basis set for C and O atoms and the LANL2DZ^{50–52} effective core potential for Au. Wave function stability was confirmed. We investigated the possible electronic states

of both the anionic and neutral structures. The spin multiplicity of $\text{Au}(\text{CO}_2)_n^-$ ($n = 2, 3$) was analyzed, calculating energies for multiplicities of 1, 3, 5, and 7. Comparative analysis of these calculated energy results indicated that the lowest energy state for $\text{Au}(\text{CO}_2)_n^-$ ($n = 2, 3$) corresponded to a singlet ground state (see Table S3 of the [supplementary material](#)). Harmonic frequency analysis was performed to confirm that the identified structures represented true minima on the potential energy surfaces and to obtain zero point energy (ZPE) corrections.

The vertical detachment energy (VDE) was theoretically calculated as the energy difference between the neutral and anionic species using the optimized geometry of the anion. The adiabatic detachment energy (ADE) was determined as the energy difference between the neutral and anion at their respective optimized geometries incorporating ZPE corrections. Based on Koopman's theorem,⁵³ the photoelectron spectra of the investigated cluster anions have been simulated at the same level of theory using the Multiwfn program.⁵⁴ In addition, the IRI⁵⁵ method, in conjunction with VMD⁵⁶ and Gnuplot⁵⁷ software, was used to visualize weak interactions. Natural population analysis (NPA) was used to examine electronic distributions in the structures.⁵⁸

RESULTS AND DISCUSSION

Photoelectron spectroscopy

Figure 1 shows the experimental photoelectron imaging spectra of Au^- and $\text{Au}(\text{CO}_2)_n^-$ ($n = 2, 3$) recorded at 355 nm (3.496 eV). The electron binding energy of the maximum of each dominant band (labeled with X) corresponds to the VDE of the ground state, which was directly measured to be 2.308 ± 0.06 for Au^- and 2.34 ± 0.06 and 2.31 ± 0.06 eV for $\text{Au}(\text{CO}_2)_2^-$ and $\text{Au}(\text{CO}_2)_3^-$, respectively. Owing to the lack of vibrational information and the indistinguishable 0–0 bands, direct measurement of the ground-state ADEs was not possible. However, these energies were estimated by determining the intersection point of a straight line along the ascending edge of the X band, considering the instrumental resolution. The ADE values for the X bands of $\text{Au}(\text{CO}_2)_n^-$ ($n = 2, 3$) were estimated to be 2.15 ± 0.06 and 2.21 ± 0.06 eV, respectively.

Comparison between experimental and theoretical results

Compared to Au^- , the spectral peaks of $\text{Au}(\text{CO}_2)_2^-$ exhibit a blue shift, with a slightly higher VDE of 40 meV, indicating the influence of CO_2 coordination. Interestingly, the VDE for $\text{Au}(\text{CO}_2)_3^-$ decreases slightly relative to $\text{Au}(\text{CO}_2)_2^-$, potentially due to structural rearrangements or electronic redistribution as the number of CO_2 molecules increases. To interpret the experimental observations, theoretical calculations were performed at the M06–2X level of theory. Figure 2 presents the ground state structures and selected low-lying isomers of $\text{Au}(\text{CO}_2)_n^-$ ($n = 2, 3$). The isomers are labeled as ABCD in Fig. 2 and arranged in order of increasing energy. The neutral structures corresponding to 2A and 3A are 2N-A and 3N-A. These anionic isomers are categorized into chemisorbed and physisorbed types. Previous studies on $\text{Au}(\text{CO}_2)_n^-$ have shown that both types coexist in AuCO_2^- , with chemisorbed isomers being more stable.^{14,45} Furthermore, only $\text{Au}(\text{CO}_2)_n^-$ ($n = 2, 3$) isomers

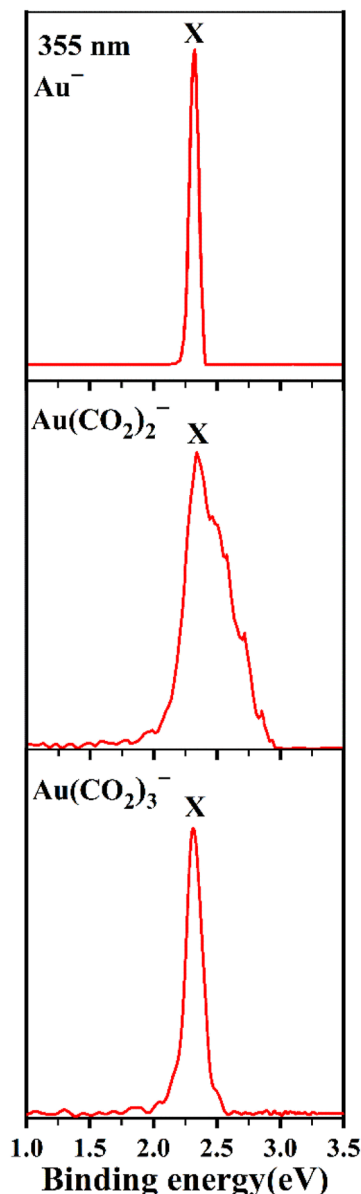


FIG. 1. Photoelectron spectra of Au^- and $\text{Au}(\text{CO}_2)_n^-$ ($n = 2, 3$) at 355 nm (3.496 eV).

exhibiting chemisorption characteristics were detected.³⁶ Interestingly, our study not only identified isomers of the physisorbed structure of $\text{Au}(\text{CO}_2)_n^-$ ($n = 2, 3$) but also determined this structure to be the lowest in energy. There are differences between our experimental methods and those employed by Weber. In particular, Weber utilized an electron gun as the laser source,⁵⁹ whereas we used an Nd:YAG laser. This distinction in the experimental setup may account for the differing observations.

The $\text{Au}(\text{CO}_2)_2^-$ isomers 2A, 2B, and 2C (Fig. 2) exhibit distinct interaction characteristics between the CO_2 molecules and

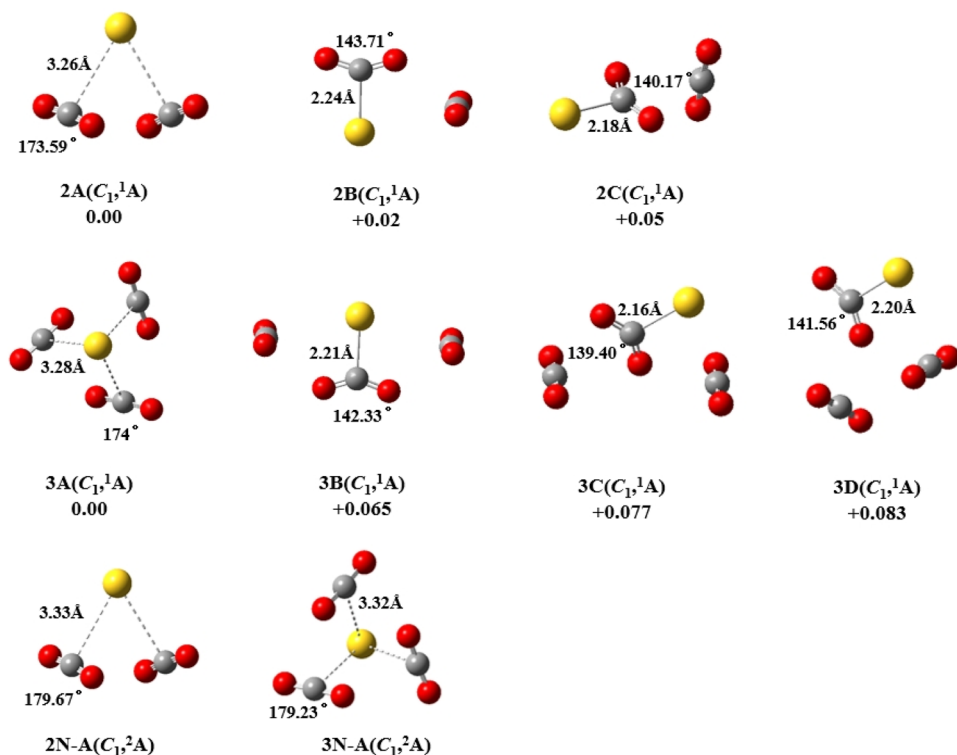


FIG. 2. Structures of the low lying isomers of Au(CO₂)_n⁻ ($n = 2, 3$) and the neutral 2N-A and 3N-A, calculated at the M06-2X/C, O/6-311G+(3df)/Au/LANL2DZ level of theory (Au, yellow; carbon, gray; and oxygen, red). The symmetry, electronic state, relative energy (eV), bond length (Å), and bond angle (in degrees) are provided.

the Au atom. In structure 2A, no considerable bonding interaction exists between the Au atom and the CO₂ molecules. The two CO₂ molecules remain independent, displaying characteristics of physical adsorption primarily driven by weak van der Waals forces. In contrast, both 2B and 2C structures show a coordination bond forming between one CO₂ molecule and the Au atom through its carbon atom. This bond results in a noticeable bending of the O–C–O angle, signifying considerable geometric distortion and indicating features of chemical adsorption. The bond length between Au and C in chemisorption is shorter than in physisorption. However, in structures 2B and 2C, the second CO₂ molecule

retains an approximately linear geometry, stabilizing it through physisorption.

In the 3A isomer (Fig. 2), the Au atom forms a trigonal pyramidal structure with the three carbon atoms, with the Au atom at the apex and the three CO₂ molecules distributed below. No considerable bonding interaction exists between the Au atom and the CO₂ molecules. The three CO₂ molecules remain independent and well separated, with relatively large intermolecular distances and no considerable bending in the O–C–O angles, similar to the 2A structure. Conversely, in the remaining three isomers, the Au atom forms a coordination bond with one CO₂ molecule, resulting in

TABLE I. Comparison of the O–C–O bond angles and Au–C bond lengths in Au(CO₂)_n⁻⁰ ($n = 2, 3$).

| Isomer | O–C–O angle (°) | Au–C bond length (Å) |
|--------|-----------------|----------------------|
| 2A | 173.59 | 3.26 |
| 2B | 143.71 | 2.24 |
| 2C | 140.17 | 2.18 |
| 3A | 174.00 | 3.28 |
| 3B | 142.33 | 2.21 |
| 3C | 139.40 | 2.16 |
| 3D | 141.56 | 2.20 |
| 2N-A | 179.67 | 3.33 |
| 3N-A | 179.63 | 3.32 |

TABLE II. Comparison of experimental and calculated VDE and ADE values of the three lowest-energy isomers for Au(CO₂)_n⁻ ($n = 2, 3$).

| Cluster | Isomer | ΔE | VDE | | ADE | |
|---------|--------|-------|---------|-------|---------|-------|
| | | | Expt. | Calc. | Expt. | Calc. |
| $n = 2$ | 2A | 0 | | 2.17 | | |
| | 2B | 0.02 | 2.34(6) | 3.10 | 2.15(6) | 2.10 |
| | 2C | 0.05 | | 3.23 | | |
| $n = 3$ | 3A | 0 | | 2.33 | | |
| | 3B | 0.065 | 2.31(6) | 3.37 | 2.21(6) | 2.25 |
| | 3C | 0.077 | | 3.47 | | |
| | 3D | 0.083 | | 3.34 | | |

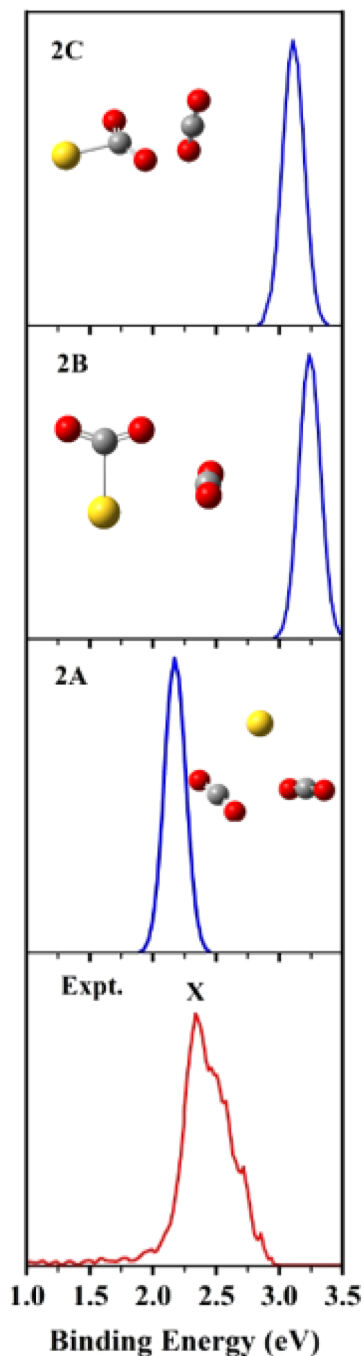


FIG. 3. Comparison of experimental 355 nm photoelectron spectra (bottom rows) of $\text{Au}(\text{CO}_2)_2^-$ to the simulated spectra of the low-lying isomers (top rows). Structures are embedded on the side.

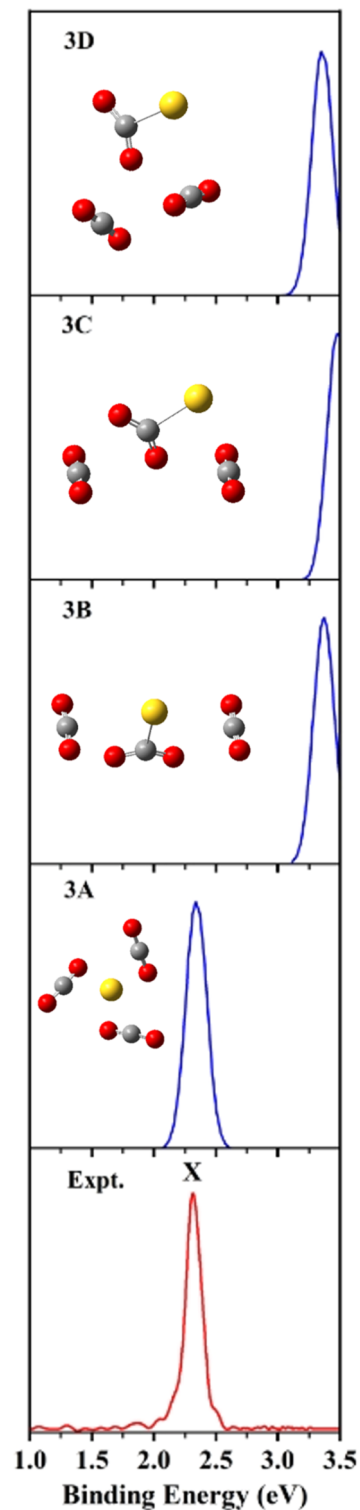


FIG. 4. Comparison of experimental 355 nm photoelectron spectra (bottom rows) of $\text{Au}(\text{CO}_2)_3^-$ to the simulated spectra of the low-lying isomers (top rows). Structures are embedded on the side.

a pronounced bending of the O–C–O angle of the CO_2 . In these cases, the Au–C distance is relatively short, while the remaining two CO_2 molecules, positioned on different planes or sites, do not form coordination bonds with the Au atom. The O–C–O angles remain

nearly linear, and the Au–C distances are comparatively longer, resembling the characteristics of structures 2B and 2C.

A key characteristic of CO₂ activation and reduction by transition metals is the bending of the O–C–O angle and the variation in bond length between the transition metal and the carbon atom.⁶⁰ In the calculated structures presented in Fig. 2 and Table I, the O–C–O bond angles in the physisorption structures are considerably larger than those in the chemisorption structures. Furthermore, the bond lengths between the Au and C atoms in the physisorbed structure are noticeably longer than those in the chemisorbed structure. In the physisorbed anion structure of Au(CO₂)₂[−], the O–C–O angles of both CO₂ molecules are 173.59°, and the Au–C bond lengths are each 3.26 Å. The O–C–O angles of the other two chemisorbed anionic structures are 143.71° and 140.17°, with the corresponding bond lengths of 2.18 and 2.24 Å. Similarly, in the physisorbed anionic structure of Au(CO₂)₃[−], all three O–C–O angles are 174°, and the bond lengths between Au and the three carbon atoms are all 3.28 Å. In the three isomers of the chemisorbed anions, the O–C–O angles range from 139.4° to 142.33°, and the Au–C bond lengths range from 2.16 to 2.21 Å. These findings indicate that CO₂ is activated during chemisorption, while it remains unactivated

in physisorption. The experimental Au(CO₂)₂[−] spectra show a significantly wider feature, probably caused by the structural change from anionic to neutral, as shown in Fig. 2, where the neutral structure has an Au–C bond length of 2.33 Å, which is an increase of 0.07 Å over the anionic structure.

For Au(CO₂)₂[−], the lowest-lying isomer is 2A, followed by 2B and 2C, with energies higher by 0.02 and 0.05 eV, respectively. As shown in Table II, the calculated VDE and ADE for isomer 2A (2.17 and 2.10 eV) agree well with the experimental results (2.34 and 2.15 eV), suggesting that 2A is the primary contributor to the experimental spectrum. In contrast, isomers 2B and 2C have VDE values of 3.1 and 3.23 eV, which fall outside the observed experimental range (the experimental spectrum does not exhibit any peak beyond 3.0 eV). As shown in Fig. 3, the simulated spectrum of isomer 2A aligns well with the experimental spectrum, supporting 2A as the dominant isomer. Although the simulated spectra of 2B and 2C do not match the experimental data, minor contributions from these isomers under varying conditions cannot be entirely ruled out.

For Au(CO₂)₃[−], the most stable isomer is 3A. Isomer 3B is 0.065 eV higher in energy than 3A. Isomers 3C and 3D are

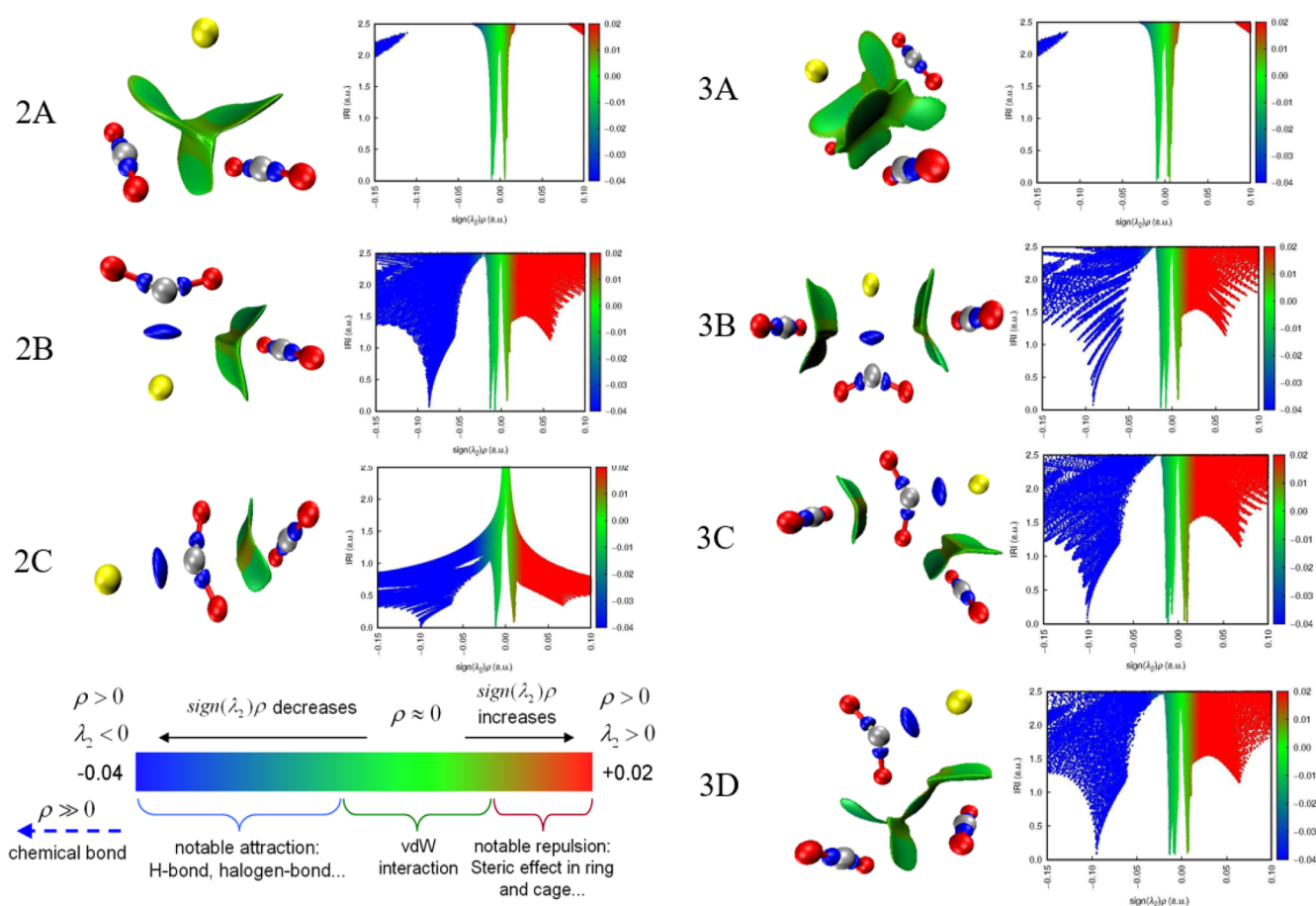


FIG. 5. Weak interaction analysis of Au(CO₂)_n[−] (n = 2, 3) anions.

0.077 and 0.083 eV higher in energy than 3A, respectively. The calculated VDE and ADE values for the most stable isomer 3A are 2.33 and 2.25 eV, which closely match the experimental values of 2.31 and 2.21 eV. In contrast, the VDE values for isomers 3B, 3C, and 3D are 3.37, 3.47, and 3.34 eV, respectively—considerably higher than the experimental peak. Thus, 3A appears to be the primary contributor to the experimental spectrum. The absence of peaks above 3.0 eV corresponding to 3B, 3C, and 3D in the experimental spectrum may result from experimental conditions that prevented the detection of these isomers (Fig. 4). The absence of these isomers in the experimental data may be attributed to the measurement range, signal intensity of the photoelectron spectroscopy, and the resolution of the experimental setup. These factors could have contributed to the inability to clearly resolve the signals of the isomers.

Transitioning from the 2A to the 3A system, the addition of an extra ligand resulted in minimal changes to the CO₂ structure, the distance between the Au and C atoms, and the adsorption dynamics of CO₂ onto the Au atoms. However, a notable change is observed in the spatial arrangement of CO₂ in the system, likely attributed to the increased number of ligands.

The IRI⁵⁵ method, developed by Lu *et al.*, offers a unique capability to visualize atomic interactions. It effectively differentiates between chemical bond regions and weak interaction regions through isosurfaces. By analyzing the IRI isosurface and scatter maps, the nature of the interactions can be readily discerned. As shown in Fig. 5, the isosurface for structures 2A and 3A revealed a distinct green area between Au and CO₂, indicating a weak interaction zone. The van der Waals interaction is evident in the scatter map as green spikes ranging from -0.010 to 0.008 a.u. For other structures, the blue regions indicate the formation of a stronger interaction, likely a coordination bond between one CO₂ molecule and the Au atom. These stronger interactions, indicative of chemical adsorption, are represented by blue spikes in the scatter map ranging from -0.100 to -0.080 a.u. This analysis aligns with the results obtained from other methods, reinforcing the conclusion that the Au(CO₂)_n⁻ (*n* = 2, 3) systems are primarily stabilized by weak van der Waals forces, or physical adsorption, rather than strong chemical bonding.

NPA was used to visualize the charge distribution changes in structures 2A and 3A. The natural charge data presented in Table III reveal that the Au atom in 2A and 3A has charges of 0.9449 and 0.9431, respectively, indicating that electron density

primarily accumulates on the Au atom. The slight differences in the valence electron count (11.943 and 11.941) suggest that the Au atom participates in similar electronic interactions in both systems. From 2A to 3A, the overall changes in electron distribution are minimal, with only slight variations in the charges of all atoms, particularly Au, C, and O. The interaction between the Au atom and the adsorbed molecules appears weak because the valence electron count of Au remains nearly unchanged. These findings further support the conclusion that the interaction between Au and CO₂ is dominated by van der Waals forces, consistent with physical adsorption.

CONCLUSION

This study presents a comprehensive investigation of Au(CO₂)_n⁻ (*n* = 2, 3) using photoelectron spectroscopy and quantum chemical calculations to elucidate the electronic and geometric structures of these complexes. The simulated photoelectron spectra of the physisorption anions 2A and 3A show good agreement with experimental results. Furthermore, the IRI method and NPA were applied to investigate the weak interactions and electronic distributions of Au(CO₂)_n⁻ (*n* = 2, 3). The results indicate that the ground-state structures of 2A and 3A are primarily stabilized by weak van der Waals forces, or physical adsorption, rather than strong chemical bonding. This research not only deepens our understanding of the physical and chemical adsorption processes in the Au(CO₂)_n⁻ (*n* = 2, 3) system but also lays the foundation for future investigations into the adsorption mechanisms of various molecules on metal surfaces. These findings provide theoretical support for optimizing related catalyst designs and applications.

SUPPLEMENTARY MATERIAL

The [supplementary material](#) encompasses relative energy differences of Au(CO₂)_n⁻ (*n* = 2, 3) calculated using various functionals and basis sets (Table S1), comparison of calculated and experimental VDE values for Au(CO₂)_n⁻ (*n* = 2, 3) using various functionals and basis sets (Table S2), and spin multiplicities and corresponding energies for Au(CO₂)₂⁻ (Table S3).

ACKNOWLEDGMENTS

This work was supported by the National Natural Science Foundation of China (Grant Nos. 21976049, 12004094, 12004095, and 22273101), the Natural Science Foundation of Hebei Province (Grant Nos. B2021402006 and A2024402007), the Funded By Science and Technology Project of Hebei Education Department (Grant No. BJK2022057), and the Education and Teaching Reform Project of Hebei Province (Grant No. 2023GJJG262). The authors gratefully acknowledge the Dalian Coherent Light Source (DCLS) for support and assistance.

AUTHOR DECLARATIONS

Conflict of Interest

The authors have no conflicts to disclose.

TABLE III. Natural population analysis (NPA) charges of the Au(CO₂)_n⁻ (*n* = 2, 3) species calculated at the M06-2X/C, O/6-311G+(3df)/Au/LANL2DZ level.

| Species | Atom | Charge | Valence |
|---------|------|-----------|---------|
| 2A | Au | -0.944 94 | 11.943 |
| | C | 1.075 66 | 2.876 |
| | O | -0.541 96 | 6.508 |
| | O | -0.561 23 | 6.527 |
| 3A | Au | -0.943 06 | 11.941 |
| | C | 1.088 40 | 2.870 |
| | O | -0.541 15 | 6.507 |
| | O | -0.566 35 | 6.530 |

Author Contributions

Z.G. and S.D. contributed equally to this work.

Zonghui Guo: Writing – original draft (equal). **Shihu Du:** Writing – review & editing (equal). **Wei Huang:** Writing – review & editing (equal). **Wenbao Zhao:** Writing – review & editing (equal). **Haiyan Han:** Writing – review & editing (equal). **Zhi Zhao:** Writing – review & editing (equal). **Yongliang Yan:** Writing – review & editing (equal). **Zhihui Fan:** Writing – review & editing (equal). **Ruili Shi:** Writing – review & editing (equal). **Hua Xie:** Writing – review & editing (supporting). **Ling Jiang:** Writing – review & editing (equal).

DATA AVAILABILITY

The data that support the findings of this study are available from the corresponding authors upon reasonable request.

REFERENCES

- L. G. Dodson, M. C. Thompson, and J. M. Weber, “Characterization of intermediate oxidation states in CO₂ activation,” *Annu. Rev. Phys. Chem.* **69**, 231 (2018).
- A. Álvarez *et al.*, “CO₂ activation over catalytic surfaces,” *ChemPhysChem* **18**, 3135 (2017).
- N. Todoroki, H. Tsurumaki *et al.*, “Surface atomic arrangement dependence of electrochemical CO₂ reduction on gold: Online electrochemical mass spectrometric study on low-index Au (*hkl*) surfaces,” *ACS Catal.* **9**(2), 1383 (2019).
- R. Wang *et al.*, “Gas-phase CO₂ activation with single electrons, metal atoms, clusters, and molecules,” *J. Energy Chem.* **63**, 130 (2021).
- A. J. Hunt *et al.*, “Generation, capture, and utilization of industrial carbon dioxide,” *ChemSusChem* **3**, 306 (2010).
- S. Y. Tang *et al.*, “Ligand-controlled CO₂ activation mediated by cationic titanium hydride complexes, [LTiH]⁺ (L = Cp₂, O),” *Chem. - Eur. J.* **21**, 8483 (2015).
- Q. Li *et al.*, “Activation of CO₂ by alkaline-earth metal hydrides: Matrix infrared spectra and DFT calculations of HM(O₂CH) and (MH₂)(HCOOH) complexes (M = Sr, Ba),” *Inorg. Chem.* **60**, 11466 (2021).
- H. Zheng *et al.*, “Spectroscopic identification of transition-metal M[η²-(O,O)C] species for highly-efficient CO₂ activation,” *J. Phys. Chem. Lett.* **12**, 472 (2020).
- G. Liu *et al.*, “The metallo-formate anions, M(CO₂)⁻, M = Ni, Pd, Pt, formed by electron-induced CO₂ activation,” *Phys. Chem. Chem. Phys.* **21**, 10955 (2019).
- A. Iskra *et al.*, “Infrared spectroscopy of gas-phase M⁺(CO₂)_n (M = Co, Rh, Ir) ion–molecule complexes,” *J. Phys. Chem. A* **121**, 133 (2017).
- S.-G. Wang *et al.*, “Factors controlling the interaction of CO₂ with transition metal surfaces,” *J. Phys. Chem. C* **111**, 16934 (2007).
- Y. Zhou *et al.*, “Generation and characterization of the charge-transferred diradical complex CaCO₂ with an open-shell singlet ground state,” *J. Am. Chem. Soc.* **144**, 8355 (2022).
- M. C. Thompson and J. M. Weber, “Infrared photodissociation spectra of [Sn(CO₂)_n]⁻ cluster ions,” *J. Phys. Chem. A* **122**, 3772 (2018).
- X. Zhang *et al.*, “Photoelectron spectroscopic and computational study of (M–CO₂)⁻ anions, M = Cu, Ag, Au,” *J. Chem. Phys.* **143**, 174305 (2015).
- B. J. Knurr and J. M. Weber, “Structural diversity of copper–CO₂ complexes: Infrared spectra and structures of [Cu(CO₂)_n]⁻ clusters,” *J. Phys. Chem. A* **118**, 10246 (2014).
- M. C. Thompson, L. G. Dodson, and J. M. Weber, “Structural motifs of [Fe(CO₂)_n]⁻ clusters (n = 3–7),” *J. Phys. Chem. A* **121**, 4132 (2017).
- Y. Liu *et al.*, “Multistate dynamics and kinetics of CO₂ activation by Ta⁺ in the gas phase: Insights into single-atom catalysis,” *J. Am. Chem. Soc.* **146**, 14182 (2024).
- A. W. Castleman, Jr. and R. G. Keese, “Gas-phase clusters: Spanning the states of matter,” *Science* **241**, 36 (1988).
- X. Kong *et al.*, “Reactions of 3d transition metal hydride cations with CO₂,” *Comput. Theor. Chem.* **1222**, 114052 (2023).
- D. Yang *et al.*, “Infrared photodissociation spectroscopic and theoretical study of [Co(CO₂)_n]⁺ clusters,” *Chin. J. Chem. Phys.* **32**, 223 (2019).
- Y. Watabe *et al.*, “Theoretical calculations of photoelectron spectrum of (Au–CO₂)⁻ anion,” *Comput. Theor. Chem.* **1140**, 56 (2018).
- X. Xing *et al.*, “Reactions between M⁺ (M = Si, Ge, Sn and Pb) and benzene in the gas phase,” *Rapid Commun. Mass Spectrom.* **17**, 1743 (2003).
- X. Zhao *et al.*, “Reactions of first-row transition metal ions with propargyl alcohol in the gas phase,” *Rapid Commun. Mass Spectrom.* **15**, 1317 (2001).
- J. Mascetti, F. Galan, and I. Papai, “Carbon dioxide interaction with metal atoms: Matrix isolation spectroscopic study and DFT calculations,” *Coord. Chem. Rev.* **190**, 557 (1999).
- N. R. Walker, R. S. Walters, and M. A. Duncan, “Frontiers in the infrared spectroscopy of gas phase metal ion complexes,” *New J. Chem.* **29**, 1495 (2005).
- J. M. Weber, “The interaction of negative charge with carbon dioxide—insight into solvation, speciation and reductive activation from cluster studies,” *Int. Rev. Phys. Chem.* **33**, 489 (2014).
- Z. Zhao *et al.*, “Reactions of copper and silver cations with carbon dioxide: An infrared photodissociation spectroscopic and theoretical study,” *J. Phys. Chem. A* **121**, 3220 (2017).
- Y. Yang, G. Wang, and M. Zhou, “Infrared spectroscopy of [M(CO₂)_n]⁺ (M = Ca, Sr, and Ba; n = 1–4) in the gas phase: Solvation-induced electron transfer and activation of CO₂,” *J. Phys. Chem. A* **128**, 618 (2024).
- A. M. Ricks, A. D. Brathwaite, and M. A. Duncan, “IR spectroscopy of gas phase V(CO₂)_n⁺ clusters: Solvation-induced electron transfer and activation of CO₂,” *J. Phys. Chem. A* **117**, 11490 (2013).
- N. R. Walker *et al.*, “Growth dynamics and intracluster reactions in Ni⁺(CO₂)_n complexes via infrared spectroscopy,” *J. Chem. Phys.* **121**, 10498 (2004).
- R. S. Walters *et al.*, “Infrared photodissociation spectroscopy of mass-selected Al⁺(CO₂)_n and Al⁺(CO₂)_nAr clusters,” *J. Phys. Chem. A* **107**, 7396 (2003).
- J. B. Jaeger *et al.*, “Infrared photodissociation spectroscopy of Si⁺(CO₂)_n and Si⁺(CO₂)_nAr complexes—Evidence for unanticipated intracluster reactions,” *Can. J. Chem.* **82**, 934 (2004).
- G. Gregoire, J. Velasquez, and M. A. Duncan, “Infrared photodissociation spectroscopy of small Fe⁺–(CO₂)_n and Fe⁺–(CO₂)_nAr clusters,” *Chem. Phys. Lett.* **349**, 451 (2001).
- C. T. Scurlock, S. H. Pullins, and M. A. Duncan, “Photodissociation spectroscopy of Ca⁺–CO₂,” *J. Chem. Phys.* **105**, 3579 (1996).
- A. D. Boese *et al.*, “The infrared spectrum of Au⁻.CO₂,” *J. Chem. Phys.* **122**, 154301 (2005).
- B. J. Knurr and J. M. Weber, “Solvent-driven reductive activation of carbon dioxide by gold anions,” *J. Am. Chem. Soc.* **134**, 18804 (2012).
- M. C. Thompson and J. M. Weber, “Enhancement of infrared activity by moving electrons through bonds—The case of CO₂ anion and carboxylate,” *Chem. Phys. Lett.* **683**, 586 (2017).
- M. C. Thompson, J. Ramsay, and J. M. Weber, “Solvent-driven reductive activation of CO₂ by bismuth: Switching from metalloformate complexes to oxalate products,” *Angew. Chem., Int. Ed.* **55**, 15171 (2016).
- B. J. Knurr and J. M. Weber, “Infrared spectra and structures of anionic complexes of cobalt with carbon dioxide ligands,” *J. Phys. Chem. A* **118**, 4056 (2014).
- B. J. Knurr and J. M. Weber, “Interaction of nickel with carbon dioxide in [Ni(CO₂)_n]⁻ clusters studied by infrared spectroscopy,” *J. Phys. Chem. A* **118**, 8753 (2014).
- M. C. Thompson, J. Ramsay, and J. M. Weber, “Interaction of CO₂ with atomic manganese in the presence of an excess negative charge probed by infrared spectroscopy of [Mn(CO₂)_n]⁻ clusters,” *J. Phys. Chem. A* **121**, 7534 (2017).

- ⁴²G. B. S. Miller *et al.*, “Spectroscopic identification of a bidentate binding motif in the anionic magnesium–CO₂ complex ([ClMgCO₂][−]),” *Angew. Chem., Int. Ed.* **53**, 14407 (2014).
- ⁴³Y. Gao *et al.*, “Detecting weak interactions between Au[−] and gas molecules: A photoelectron spectroscopic and *ab initio* study,” *J. Am. Chem. Soc.* **131**, 9484 (2009).
- ⁴⁴W. Zheng *et al.*, “Anion photoelectron spectroscopy of Au[−](H₂O)_{1,2}, Au₂[−](D₂O)_{1–4}, and AuOH[−],” *Chem. Phys. Lett.* **444**, 232 (2007).
- ⁴⁵Z. Liu *et al.*, “Synergetic electron donation and back-donation interactions in (Au–CO₂)[−] complex: A joint anionic photoelectron velocity-map imaging spectroscopy and theoretical investigation,” *Chem. Phys. Lett.* **803**, 139845 (2022).
- ⁴⁶Z. Qin, X. Wu, and Z. Tang, “Note: A novel dual-channel time-of-flight mass spectrometer for photoelectron imaging spectroscopy,” *Rev. Sci. Instrum.* **84**, 066108 (2013).
- ⁴⁷M. J. Frisch *et al.*, *Gaussian 09, Revision B. 01*, Gaussian, Inc., Wallingford, CT, 2009.
- ⁴⁸Y. Zhao and D. G. Truhlar, “The M06 suite of density functionals for main group thermochemistry, thermochemical kinetics, noncovalent interactions, excited states, and transition elements: Two new functionals and systematic testing of four M06-class functionals and 12 other functionals,” *Theor. Chem. Acc.* **120**, 215 (2008).
- ⁴⁹R. Krishnan *et al.*, “Self-consistent molecular orbital methods. XX. A basis set for correlated wave functions,” *J. Chem. Phys.* **72**, 650 (1980).
- ⁵⁰W. R. Wadt and P. J. Hay, “*Ab initio* effective core potentials for molecular calculations. Potentials for main group elements Na to Bi,” *J. Chem. Phys.* **82**, 284 (1985).
- ⁵¹P. J. Hay and W. R. Wadt, “*Ab initio* effective core potentials for molecular calculations. Potentials for K to Au including the outermost core orbitals,” *J. Chem. Phys.* **82**, 299 (1985).
- ⁵²P. J. Hay and W. R. Wadt, “*Ab initio* effective core potentials for molecular calculations. Potentials for the transition metal atoms Sc to Hg,” *J. Chem. Phys.* **82**, 270 (1985).
- ⁵³J. Akola *et al.*, “Photoelectron spectra of aluminum cluster anions: Temperature effects and *ab initio* simulations,” *Phys. Rev. B* **60**, R11297 (1999).
- ⁵⁴T. Lu and F. Chen, “Multiwfn: A multifunctional wavefunction analyzer,” *J. Comput. Chem.* **33**, 580 (2012).
- ⁵⁵T. Lu and Q. Chen, “Interaction region indicator: A simple real space function clearly revealing both chemical bonds and weak interactions,” *Chem.: Methods* **1**, 231 (2021).
- ⁵⁶W. Humphrey, A. Dalke, and K. Schulten, “Vmd: Visual molecular dynamics,” *J. Mol. Graphics* **14**, 33 (1996).
- ⁵⁷P. K. Janert, *Gnuplot in Action: Understanding Data with Graphs* (Manning Publications, 2016).
- ⁵⁸E. D. Glendening, C. R. Landis, and F. Weinhold, “Natural bond orbital methods,” *WIREs Comput. Mol. Sci.* **2**, 1 (2011).
- ⁵⁹J. M. Weber, “A pulsed ion source for the preparation of metal containing cluster anions using supersonic entrainment of laser vaporized metal,” *Rev. Sci. Instrum.* **76**, 043301 (2005).
- ⁶⁰E. Lim *et al.*, “Anionic activation of CO₂ via (M_n–CO₂)[−] complex on magic-numbered anionic coinage metal clusters M_n[−] (M = Cu, Ag, Au),” *J. Phys. Chem. A* **125**, 2243 (2021).